Modeling the generation and propagation of rain-triggered landslides

Rodriguez-Diaz Andrés[1]

[1]Master Student, Territories and Cities Area, School of Applied Sciences and Engineering, EAFIT University, Medellín, Colombia.

*Correspondencia del autor : acrodrigud@eafit.edu.co

Abstract

Slope stability is of great importance when the associated hazard implies a risk of human and economic losses. When a morphodynamic process materializes, there is a possibility that it may evolve into a debris and mudflow, especially when the mobilized mass is large and the phenomenon occurs in mountainous or steeply sloping terrain, where the soil mass may be channeled through watercourses or low-lying areas of the landform.

Currently, the numerical modeling of such landslide phenomena is mainly performed using limit equilibrium or finite element methods. However, these approaches present major limitations when dealing with large deformations. For example, the finite element method is constrained when oscillations between tensile and compressive stresses are generated. In addition, the discretized elements must remain connected; otherwise, the analysis fails to converge.

This research proposes to model the initiation and propagation of a rain-induced, large-deformation landslide. The modeling is structured in two stages: i) simulation of transient rainfall and infiltration using FEM (Finite Element Method), to generate conditions where convergence cannot be reached before failure; ii) export of the FEM results, mainly pore pressures and stress states for each element, to serve as initial conditions in an MPM (Material Point Method) environment, where the movement of the failed mass is modeled according to the characteristics defined for an idealized slope representing natural conditions.

To achieve this objective, a review of the numerical and constitutive bases of the methods was carried out, together with a survey of previous research on the numerical modeling of large-deformation landslides using the two approaches mentioned above. Subsequently, the geometry of an idealized slope was defined to allow predictive modeling. For this purpose, rainfall data and terrain parameters were selected from existing information for the Greater Medellín area and the Aburrá Valley in Colombia.

For the rainfall input, thresholds defined by the Early Warning System of Medellín and the Aburrá Valley (SIATA), a local hazard and risk monitoring agency, were used. A rainfall threshold can be defined, in simplified terms, as the boundary between rainfall events that can potentially trigger mass movements, usually combining data on antecedent and triggering rainfall (90-day and 7-day windows in the SIATA case). For this study, three particular threshold scenarios were selected, producing three different combinations of antecedent and triggering rainfall.

Finally, conclusions are drawn regarding the adaptation of the two-stage modeling approach for this type of landslide. The methodology takes advantage of the computational efficiency of FEM for simulating the initiation of mass movement, and of MPM for modeling the subsequent propagation of the soil mass across the topography. The study highlights the potential benefits for risk management of using low-cost basic information (rainfall thresholds) as an alternative to traditional and more expensive monitoring instruments such as inclinometers and piezometers.

Keywords: Landslides, Finite Element Method, Material Point Method, Computational Efficiency, Rain Thresholds, Runoff Distance.

Nomenclature

ρ_s = Density of Solids
J_s = Solid Phase Flux
ϕ = Porosity
f^w = Liquid Phase Source Term
P_w = Liquid Pressure
V_s = Solid Velocity
V_w = Liquid Velocity
γ_w = Unit Weight of Water
E_s =Young's Modulus
μ = Poisson Ratio
m =Power Function Parameter
P_0 = Air Entry Pressure
σ_0 = Surface Tension
λ = Shape Parameter for the soil-water retention curve (SWRD)
Srl = Maximum Degree of Saturation
Srs = Manimun Degree of Saturation
K = Hydraulic Conductivity

1. Introduction

The study of slope stability is of particular importance when it has direct implications for economic losses and loss of human life [1]. The stability of a soil mass is strongly influenced by the increase in pore pressure, decrease in suction, and consequently the decrease in the geomechanical characteristics of a material [2], This may be directly related to the hydrological conditions of a particular area, but it will also depend on the area's topography, geomorphology, and geotechnical conditions [3]. Landslides with shallow fault surfaces and debris flows are common events in tropical and mountainous environments [4], characterized by deep weathering profiles [1]. The geomorphology of tropical or alpine environments is generally characterized by steep slopes, with trough areas that channel runoff into valleys. These trough areas can become channels for landslides and debris flows, even causing blockages in rivers, thus amplifying their destructive capacity and generating chains of disasters [5].

Mudflows and debris flows are a type of rapid mass movement involving a mixture of soil, rock, vegetation and water, dragging, eroding, and displacing a large volume of material in their path[6], flowing through valleys or depressions in the terrain. Mudslides and debris flows are widespread phenomena worldwide, but some countries have higher rates of occurrence, such as Nepal, Japan, China, Brazil, and Italy[1]. China has data and reports of at least one thousand (1,000) deaths annually and approximately four billion (4,000) dollars in damages and losses per year[7]. One of the factors that most influences the occurrence of landslides is soil saturation caused by rain. Therefore, empirical and numerical methods have been developed for the prediction and early warning of landslides, such as rainfall thresholds[8], probability of exceedance [9] and spatial and temporal analyses of landslide occurrence, including more factors in the models [10]. Another determining factor in the generation of landslides and their transformation into mudflows and debris flows is the associated geology, bearing in mind that, based on the history of geological formation and modifications to the environment, the variability of the intrinsic characteristics of a material is high both vertically and horizontally [11].

The analysis and modeling of the phenomena mentioned so far is not a new topic, however, there have been significant developments in recent decades. In 1967, Whitman and Bailey mentioned how productive it could be to perform slope stability analyses using a computing unit [12], At that time, this expression preceded the study of slopes using computational analysis. One of the first and most frequently used methodologies falls within the category of limit equilibrium analysis methods. These are characterised by their reliance on the concept of a safety factor, which considers the relationship between the shear strength of the soil mass and the shear stress acting on it. This implicitly treats the soil as a ductile material [12]. Limit equilibrium methods fundamentally seek to find the critical surface, which presents the lowest ratio between resistance offered and acting shear forces. In general, analysis methods can be divided into infinite slope analysis or

segment methods.

A subsequent development corresponds to analysis methods that include stresses and deformations in numerical models, a topic mainly associated with finite element methods, which, although not the only ones in existence, have become widely used for slope stability analysis since at least the 1960s [12]. One of the first advantages identified in this method of analysis with respect to the aforementioned limit equilibrium analysis is that it is not necessary to assume or know the shape of the failure, since it is generated in areas where the resistance is exceeded [13]. With this approach, the finite element method has become a potential way of solving slope stability problems with respect to traditional methodologies. This method has been developed from several approaches, one of which is reduction methods (SMR or SRF), another approach is gravity increase (GIM), with numerical results quite similar to those mentioned initially, and a third approach corresponding to finite element limit analysis (FELA) [14].

Despite the advantages, developments, and extensive documentation currently available for the finite element method, it is not capable of reproducing the behavior when a soil mass is subjected to high deformations [15], Additionally, the elements must remain joined, and calculations become more complex when deformations are irregular. To overcome this problem, the material point method has emerged, involving the generation of a discretisation mesh and calculation of stresses at Gauss points (elastic or plastic) to determine deformations and displacements in the medium. Until stresses and deformations are calculated at the nodes, the material point method (MPM) does not differ greatly from the finite element method (FEM). However, in MPM, the mesh returns to its original position after deformation, while the material points occupy a new position. Another issue that the MPM seeks to address is the oscillation of compressive and tensile stresses, as this type of behaviour is difficult to model in soil mechanics. Additionally, the distances travelled by a soil mass can be modelled from a given geoform or surface, in either 2D or 3D. MPM simulations can also quantify the increase in interstitial pressures during mass movement events, making the material point method a powerful tool for modelling high deformations.

2. Background

For many decades, finite element analysis has been considered one of the main methods for performing numerical analysis in engineering problems in general. However, it generates problems in the analysis of very large deformations [16]. As for the initial contributions to the material point method, authors such as [17] MPM emerged in the 1960s with research on the particle-in-cell method by Harlow and Meixner (1961) [18] mainly applied to fluids, where the entire space occupied by the fluid is discretized in an Eulerian mesh and particles in a Lagrangian mesh. The MPM method is configured as an extension or modification of the particle-in-cell method, where deformations are calculated at material points and

the values obtained in the computational background mesh are omitted [19].During the development of the method, some drawbacks were observed, such as "numerical noise" when material points left the cells, a condition that was resolved in the work on generalized interpolation in MPM published by Bardenhagen and Kober in 2004 [20] with the inclusion of smoothed interpolation functions.

Another contribution similar to the current MPM method and to mass analysis with particle discretization was made by Sulsky in 1994 [21], Based on these issues or conditions that generate certain specific engineering problems, initially applied to fluid dynamics or multiphase flow analysis problems, but extended to other areas of knowledge, in this case geotechnics. The problems mentioned may be associated with differential particle movements, rotations, collisions between particles or solids, which generate a more complex numerical condition. In this case [21] He mentions that it is complex to implement the equations that are coupled to this type of problem under the foundation of an Eulerian environment, where basically what is measured are points, or the condition of the particle at a point in space. However, at the other extreme, a purely Lagrangian approach (where the particle is tracked) can lead to errors in the same way. Thus, Eulerian-Lagrangian and/or coupled approaches are beginning to be considered more appropriate for generating more realistic reproductions of the phenomena under analysis, where constitutive models for each specific particle are beginning to be solved.[22], From here, we begin with the use of MPM from the formulation of particle-in-cell of [23] This involves combining the fundamental and positive aspects of the Eulerian and Lagrangian descriptions of materials. The Lagrangian part uses material points, while the traditional finite element mesh, also known as the computational background mesh, is used for the Eulerian part. It is important to consider the conditions that must be met for the method to work correctly and produce consistent results. These include correctly establishing boundary conditions, extrapolating and interpolating the number of particles from the nodes to the mesh, and updating the stress [24].

The mass analysis approach with particle discretization has also been used to solve solid mechanics problems [23], for impact problems, where it has been shown that plastic deformations and tensile stresses are generated mainly on the impact surfaces. The implementation of this type of approach, which presents a Lagrangian-Eulerian description, arose with the aim of overcoming the disadvantage of mesh deformation in an FEM approach, tracing the history of the variables at the material points and not on the computational background mesh, classifying it as one of the so-called meshless methods [25].

In the field of geotechnical engineering, particularly with regard to slope stability, the material point method has gradually been implemented to enable analysis of cases involving internal shearing of rock masses, deep mass movements and transient analysis in the context of rain infiltration [26], adapting these types of methods to simple constitutive models or coupled history-dependent models [27]. In some cases, it has been possible to analyze progressive failures with fractures in brittle materials, such as the research

conducted by [28] This is the case of the brittle failure of the Aznalcollar dam, which is one of the many applications in which this particle discretization method can be used. More recently, approaches to modeling problems in geotechnical engineering have been implemented, taking advantage of the versatility and computational speed offered by FEM and the ability to model large displacements and deformations in MPM, such as in the case of evaluations of mass movement paths or runoff, with records of previous rainfall [9], [29] In some cases, the aim is to implement these methods within a risk management framework to predict the kinetic and runoff characteristics of landslides, including their speed and kinetic energy [30].

3. Two-Stage modeling scheme: FEM/MPM

Two-stage modelling of large deformations during landslides has already been proposed in some studies, for example [31] proposes an initial modeling stage using commercial finite element software to optimize computational speed in obtaining results for the transient simulation of rain infiltration, and a second stage using a material point program to simulate runoff from a landslide on an artificial slope. In order for the two-stage modeling (FEM/MPM) to be executed, it is necessary to export some results obtained from the transient modeling performed with FEM to the MPM software or code, such as coordinates, index property status, pore pressures or liquid pressures, degree of saturation, among others. This type of two-stage approach can be seen in the research carried out by [9] and [31] on artificial slopes.

These models are commonly carried out within a hydromechanical coupling framework. Initially, in FEM modeling, a mass flow condition is imposed that simulates rain infiltration, which can be done through a constant infiltration load or with specific data on the rain dynamics of the area where the landslide is analyzed or modeled, with the aim of highlighting variations in pore pressures and, consequently, changes in the stress state in the soil mass, which would generate deformations leading to a non-convergence problem in FEM. At this point, the finite element modeling is completed, since with this continuous medium it is not possible for the elements to separate. Therefore, the results are entered into MPM to perform the respective large deformation analyses. It is important to note that these types of models fall within the deterministic category and do not include the special variability of the conditions with which they are modeled. Some authors, such as [31] introduce a probabilistic analysis framework to modeling.

After transferring the information on the conditions generated and/or imposed on the slope in the finite element stage, the soil mass is discretized into material points, each of which will contain all the information (stresses, properties, deformations, density, among others) [9].The advantage of transferring information from FEM to MPM lies in the fact that both models are based on a similar mechanical environment, for example, the conservation of mass [15], That being the case, it could be said that many of the

advantages and disadvantages of finite element modeling also remain. It is important to understand that in the framework of material point modeling, there is no penetration between particles; however, there can be separation between particles, slippage, friction, among other things [22]. The material points method can be applied under a framework of fully saturated soils or multiphase media, or partially saturated soils [9]. Given that it is possible to model separate particles, it is possible to obtain more realistic results. However, for such a simulation to be truly consistent with what occurred during the mobilization of the mass, it is important to correctly establish the initial conditions and use rigorous, non-simplified formulations for modeling with the material point method.

As mentioned above, the MPM formulation is essentially based on the same theoretical principles as the finite element method, with the fundamental difference being that mass is discretised into material points. In this sense, the material points could be said to play a role similar to the Gauss integration points in FEM. The background mesh can be restored to its original condition when the solutions are generated, while the material points retain all the displacements they have undergone. According to González and Hicks (2021) [15] MPM has three fundamental steps, two of which are similar to FEM. This results in partial equivalence between the two methods. The first two steps involve mapping and integrating mechanical equations using material points rather than Gaussian points, while the second step involves solving these equations. In the third phase of MPM, the material points undergo the corresponding deformation. However, unlike in FEM, the mesh does not return to its original position.

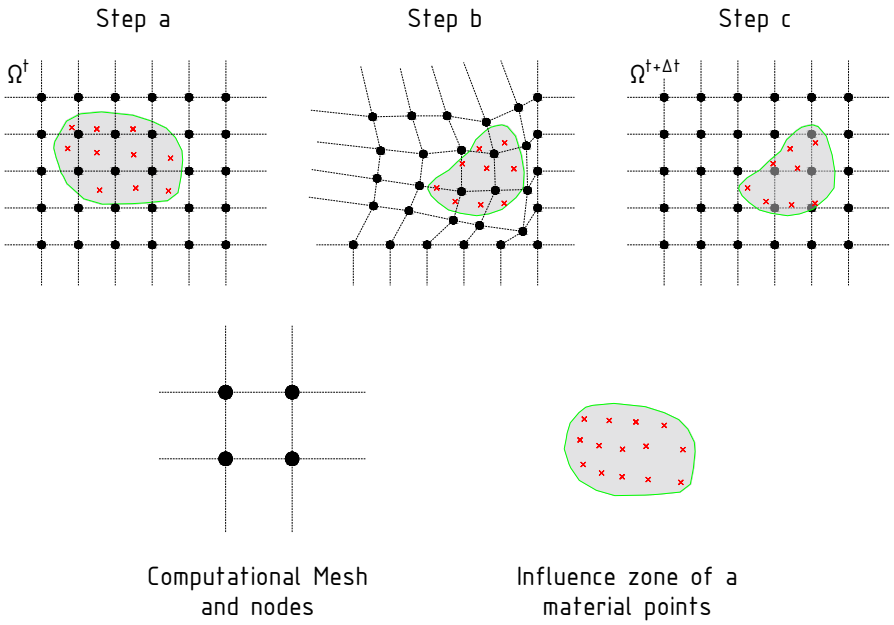

Figure 1: Secuence of MPM algorithm steps ocurring in each time step a) mapping and integration, b) solution and material point location update, and c) mesh reset. Source: González and Hicks (2021) [15]

Therefore, this research proposes a review of existing knowledge on theories and modelling of rainfall-triggered landslides, using hybrid approaches that combine the computational advantages of finite element method (FEM) and Material Point method (MPM).

4. Formulation and Theoretical Basis

Authors such as [27] have worked extensively on the development of processes in the field of geotechnics for the fully coupled (hydro-mechanical) analysis of flow-deformation models. During the research, it was found that the transient dissipation process has several considerations, such as the heterogeneous distribution of pressures on the slope, changing saturation, and deformation of the soil structure itself. As such, only a fully coupled analysis could reflect a condition close to reality in a model. It is important to mention that only in soil with very high permeability or very rigid soil would there be no noticeable change between modeling, for example, pure flow (uncoupled) and modeling under coupled flow-deformation conditions.

This chapter provides a brief overview of the theoretical and numerical basis for achieving the hydro-mechanical coupling sought in this article. To this end, it compiles the developments shown by [27] for hydro-mechanical coupling under saturated and unsaturated conditions. When a mass flow infiltrates, pore deformation is generated, which is ignored in a decoupled analysis. These deformations will be defined in terms of displacements (µ) associated with small deformations and deformation velocities.

In finite element analyses (FEM), the equations governing flow in the soil for the different phases can be presented in reduced form, as explained by [32] in the development of research on multiphase flow through saline media. The mass balance of the solid phase can be written as follows:

$$\frac{\partial}{\partial t}\left(\rho_s(1-\varphi)\right) + \nabla \cdot \mathbf{J_s} = 0 \tag{1}$$

Where:

- ρ_s = Mass of solid per unit volume of solid.
- $\mathbf{J_s}$ = Solid flux.
- φ = porosity.

Taking into account the above equation, a reduced expression for the variation in porosity can be obtained, provided that said solid flow is written as the velocity of the solids multiplied by the volumetric fraction of the solids (volume of the solids with respect to the total volume) and their density.

$$\mathbf{J_s} = \rho_s(1-\varphi)\frac{d\mu}{dt} \tag{2}$$

Subsequently, the variation in porosity (pore deformation) caused by volumetric deformation and the variation in solid density can be expressed as follows:

$$\frac{D_s\varphi}{Dt} = \frac{(1-\varphi)}{\rho_s} \cdot \frac{D_s\rho_s}{Dt} + (1-\varphi) + \nabla \cdot \left(\frac{d\mu}{dt}\right) = 0 \tag{3}$$

Additionally, the total balance of the water mass can be expressed as:

$$\frac{\partial}{\partial t}\left(\rho_w S_w \varphi\right) + \nabla \cdot \mathbf{J_w} = f^w \tag{4}$$

Where the balance is in terms of water density, degree of saturation, flow, and external source. Subsequently, if we add the solid balance to the equation, we have the following:

$$\frac{S_w\phi}{\rho_w}\frac{D_s\rho_w}{Dt} + \phi\frac{D_sS_w}{Dt} + \frac{S_w(1-\phi)}{\rho_s}\frac{D_s\rho_s}{Dt} + S_w\nabla\cdot\left(\frac{d\mu}{dt}\right) + \frac{1}{\rho_w}\nabla\cdot(\rho_w q_w) = \frac{1}{\rho_w}f^w \tag{5}$$

The equation has four (4) terms, including water compressibility, suction retention, and solid compressibility. The use of the equation determined will depend on the conditions in the field. For example, if the medium is completely saturated, the second term of the equation disappears. Additionally, if the soil is extremely rigid, the compressibility of the solid particles can be disregarded. In some scenarios, the compressibility of water can be disregarded; however, if we are dealing with very rigid soil, it cannot be disregarded.

Later in the mathematical development, the dependent variables are related to their unknowns, assuming that the flow or sources is 0. Thus, the expression for the development of water pressure for soil subjected to changes in total stress can be obtained.

$$DP_w = \frac{-S_w\frac{\partial\varepsilon_v}{\partial\sigma}d\sigma - \frac{dt}{\rho_w}\nabla\cdot(\rho_w q_w)}{\frac{\phi S_w}{K_w} + \phi\frac{dS_w}{d\rho_w} + \frac{S_w\partial\varepsilon_v}{d\rho_w}} \tag{6}$$

It is important to note that in the above equation, deformation and stress are assumed to be negative in compression. Additionally, the deformation tensor remains unchanged because any change in stress can produce deformation.

In analysis using the material points method (MPM), specifically when dealing with multiphase media as in the case evaluated in this research, the governing equations correspond to the momentum of the mixture, the momentum of the fluid, and the mass balance of the liquid phase.

The governing equations mentioned above will be presented below, taking into account the formulation developed in the research presented by [33].

The equations are expressed in terms of the velocity of both phases, in this case, solid and fluid (liquid), disregarding volumetric deformation at the granular level.

- Momentum balance of the mixture:

$$\nabla\cdot\sigma - (1-\phi)\rho_s V_S - \phi\rho_w V_w + \rho b = 0 \tag{7}$$

- Momentum balance of the fluid:

$$\nabla P - \rho_w V_w - \frac{\phi \gamma_w}{k}(V_w - V_S) + \rho_w b = 0 \tag{8}$$

- Mass balance equation for the liquid phase:

$$\dot{P} = \frac{k_w}{\phi}\left[(1-\phi)\nabla \cdot V_S + \phi \nabla \cdot V_w\right] \tag{9}$$

S and W are used as subscripts to denote the solid and liquid phases, respectively. The equations are given in terms of the density for each particular phase. Furthermore, k_w is the compressibility modulus of the liquid, ϕ is the porosity, y $\dot{P}$ represents the pressure.

5. Synthetic slope modeling

This chapter will present the fully coupled modeling of a synthetic slope under the effects of rain, showing both FEM and MPM software, the definition of the synthetic slope geometry and boundary conditions, selected geomaterials, bottom meshing, and the calculation scheme designed to obtain results.

5.1 Modeling Software

The software used for modelling is CODEBRIGHT, a program that enables fully coupled thermo-hydro-mechanical analyses and specialises in geological and geotechnical issues. This meets the modelling objectives. It was developed by the Department of Civil and Environmental Engineering at the Polytechnic University of Catalonia in Barcelona, Spain.

The software used for material point modeling (MPM) is Anura3D, an open-source program for high-strain analysis that takes into account soil-water-structure coupling and allows for the modeling of a wide range of geological problems, such as soil mass failure, liquefaction, erosion, consolidation, and impact, among others. This material point analysis software has been developed by researchers from various universities, including Deltares, the Polytechnic University of Catalonia, TU Delft, and Virginia Tech, among others.

One of the advantages of using the aforementioned software is that in both cases, the pre-processing, which basically corresponds to the definition of the geological model, its geometry, initial conditions, associated materials, computational mesh, and other aspects, can be executed in the GID software, which in the case of this research was version 10.0.6 of the program. GID is a program used for numerical simulation, analysis, and visualization of results.

Para el caso de CODEBRIGHT se puede encontrar en la página web de la Universidad Politécnica de Cataluña la información detallada para la instalación del CODEBRIGHT en la versión de GID indicada, atendiendo algunos requerimientos de sistema y programas

adicionales para el correcto funcionamiento de este. En el caso del Anura3D es necesario compilar el código fuente, preferiblemente utilizando el programa Visual Studio según las recomendaciones de los desarrollados para posteriormente realizar el ensamblaje de los archivos que permitirán modelar con el software con MPM en GID.

The post-processing corresponding to the final visualization of results was performed in the same GID environment for the case of modeling using finite element analysis (FEM) and Paraview 5.13.0 for the results of the material point method (MPM) modeling.

5.2 Initial Geometry

For the geometry to be used in the modeling, a synthetic slope is considered, which does not correspond to a real topographic profile but rather to a simplified representation of a mass of soil with a slope. The objective is to carry out modeling under the concept of plane deformation, taking the lower left corner of the model with coordinates 0,0 as the origin.

For the selection of materials, a weathering profile is defined for a fairly common igneous material in the city of Medellín and Valle de Aburra (Colombia), corresponding to the Altavista Stock, a material that develops deep soil profiles and in which landslides are very common in its upper layers. Thus, a synthetic slope model is generated with a transition between weathering horizons VI and V of the Altavista Stock. Horizon V corresponds to a completely weathered rock in which its inherited structures can still be seen. It is a material that generally has a sandy loam texture and is easily disintegrated. Horizon VI corresponds to a completely weathered soil with a mainly silty clay texture in which the structures of the parent rock are no longer visible.

The model has a length of up to 36.0 m and an elevation of up to 20.0 m. In addition, a groundwater level is established at approximately 3.0 m from the base of the model. The difference in stiffness between horizons V and VI is significant, therefore the expected behavior when inducing the fault will be the generation of a residual soil slide above horizon V.

Due to its relatively regular geometry, this synthetic slope can mainly be associated with a road embankment cut, in which adjustments are made to ensure the grade of the roads to be built and which in many cases do not have the required analyses to guarantee stability, thus triggering failures that culminate in the loss of the road embankment.

The synthetic model generated for the purpose of performing fully coupled analyses using the FEM-MPM approach mentioned in previous chapters is presented below.

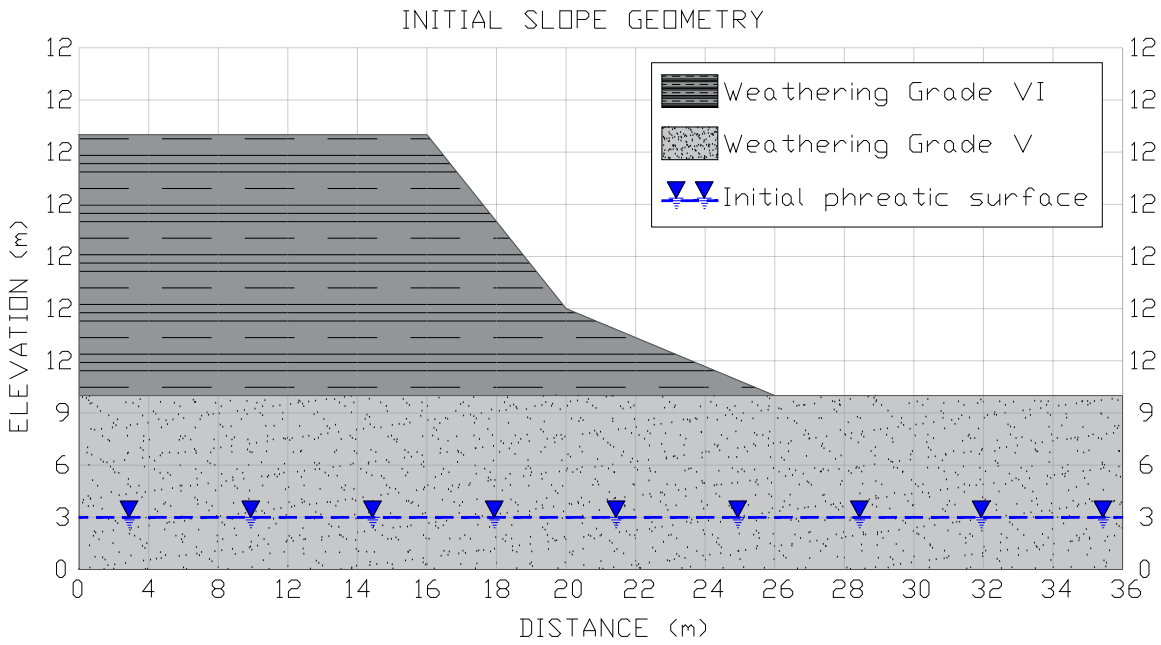

Figure 2: Initial geometry of the model
Source: Author's elaboration

5.3 Materials

As mentioned above, for the modeling covered in this research, we have chosen to select parameters typical of a weathering profile, superficially a clay loam soil, and subsequently a sandy loam soil with greater rigidity. The modeling will be carried out for a two-phase medium with a suction effect. Elastoplastic theory will be used for finite element modeling, and parameters will be defined for the soil moisture retention curve and the permeability of the different materials to be modeled.

The Table 1 shows the mechanical and hydraulic properties of the two weathering horizons selected for modeling.

5.4 Boundary conditions, computational mesh and material points definition

The kinematic restriction conditions of the proposed two-dimensional plane strain model will be shown below. For the solid phase, horizontal movement (X-axis) is prevented for the sides, and both horizontal and vertical movement (X and Y axes) is prevented for the base of the model. For the liquid phase, boundary conditions with restrictions in X on the sides and in Y on the base of the model are imposed.

To simulate initial conditions such as the water table, which is located 3.0 m from the

Table 1: *Propiedades básicas y constitutivas de los materiales a modelizar.*

Constitutive Model	**Parameter**	**Symbol**	**Unit**	**Weathering horizon**	
				V	**VI**
Linear-elastic model	Young's modulus	E_s	MPa	15	8
	Poisson ratio	μ	-	0.30	0.36
Elasto - plastic model	Power function parameter	m	-	2	2
	Fluidity = 1/viscosity	Γ_0	S^{-1} MPa^{-m}	0.01	0.01
	Effective cohesion	C	MPa	20	6
	Effective Friction angle	ϕ	°	30	25
Van Genuchten	Aire entry pressure Po	P_o	MPa	0.02	0.02
	Surface tension corresponding to the temperature at Po	σ_0	N m^{-1}	0.072	0.072
	Shape parameter for the soil-water retention curve (SWRC)	λ	-	0.2	0.2
	Minimum degree of saturation	S_{rl}	-	0	0
	Maximum degree of saturation	S_{rs}	-	1	1
Permeability	Principal direction 1	k_1	m^2	1.0E-12	1.0E-12
	Principal direction 2	k_2	m^2	1.0E-12	1.0E-12
	Principal direction 3	k_3	m^2	1.0E-12	1.0E-12

base of the model, positive liquid pressure is applied from the base of the model, decreasing to zero at the zero pore pressure line or water table (3.0 m from the base, hereafter negative liquid pressures are imposed, corresponding to suction in the interstices of the soil mass.

As shown in Figure 3 one of the boundary conditions imposed corresponds to an infiltration rate that simulates rainfall on a slope, for which rainfall data in mm is normally available from a rain gauge data set. To impose this condition in the CODEBRIGHT software (finite elements), the rainfall has been converted from mm/m^2 to a mass flow unit, in this case kg/m^2*s.As for the computational background mesh, the same configuration was used for both the models generated in the finite element analysis (FEM) and the model generated for analysis using the material point method (MPM), which is an unstructured mesh with 1.80 m triangular elements.

For the initial conditions imposed, the liquid pressure for simulating the groundwater level corresponds to a nodal variable. Therefore, it is imposed on each of the model nodes according to the simplified distribution mentioned above, with positive liquid pressures below the groundwater level and negative pressures above it.

For meshing in modeling using the material point method, the GID pre-processing system was used to generate a mesh with the same conditions. Additionally, in order to obtain better results in the soil mass breakage stage, the medium was discretized into a

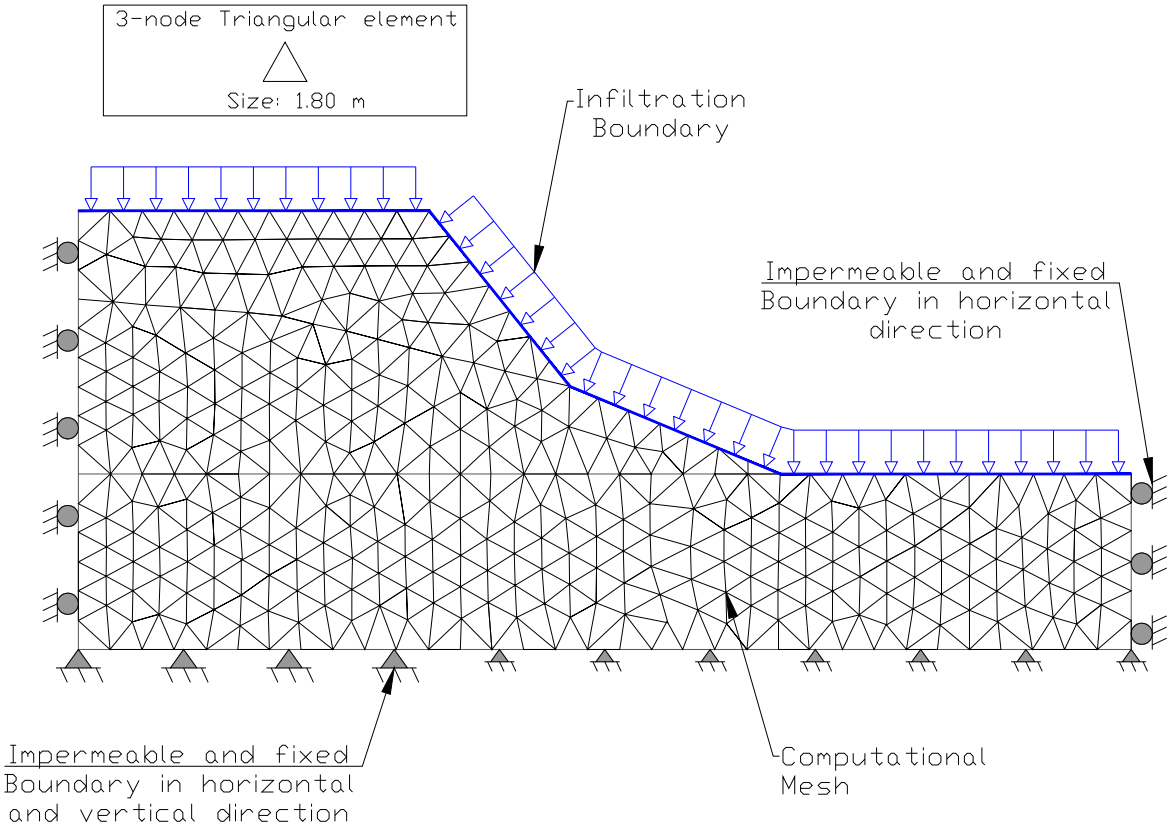

Figure 3: Boundary conditions and computational mesh
Source: Author's elaboration

higher density of material points for the material associated with Weathering Horizon V or surface materials.

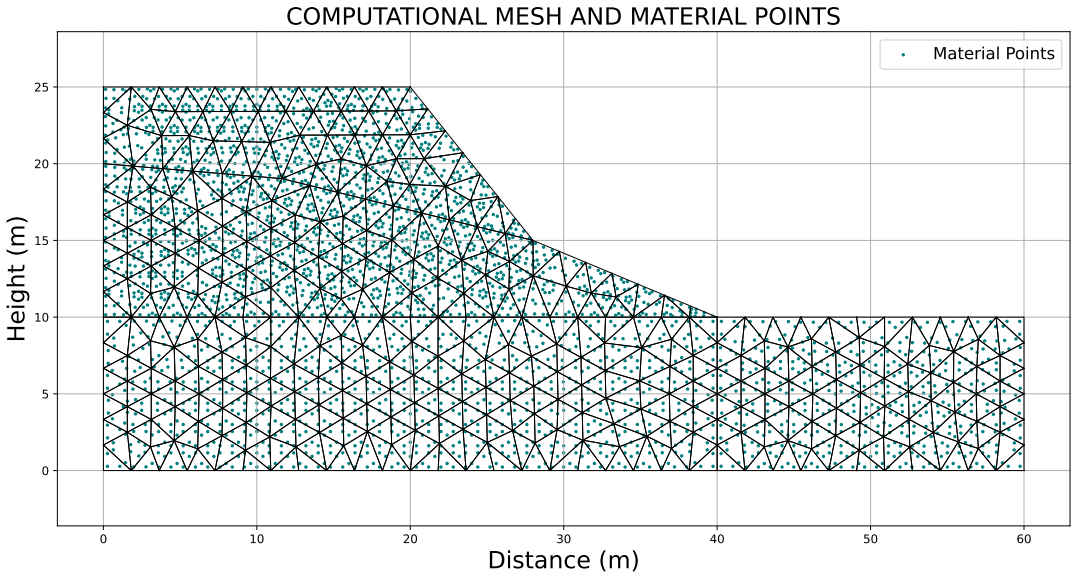

Figure 4: MPM model for a slope under rainfall infiltration.
Source: Author's elaboration

Given that this research involves modeling a multiphase medium (liquid and solid), a

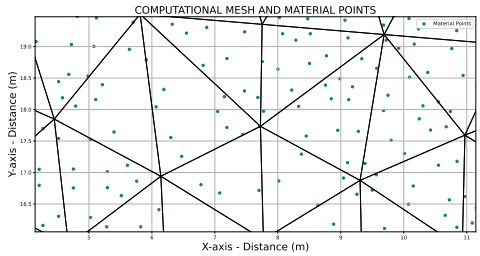

(a) Discretization of material points for Weathering Horizon VI

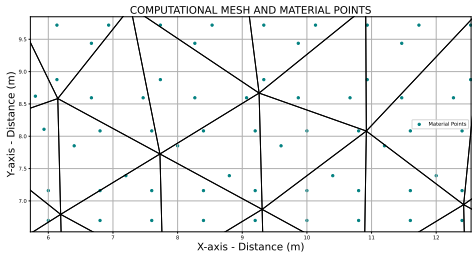

(b) Discretization of material points for Weathering Horizon V

Figure 5: Number of material points for the different horizons established in the model

visco-elasto-plastic constitutive model has been chosen for fully coupled hydro-mechanical modeling, as in the research carried out by [34] where cohesion in the soil depends on suction and matrix porosity. Regarding the hydraulic parameters for modeling, the soil moisture retention curve was used with the Van Genuchten model.

5.5 Modeling strategy / Computational scheme

The objective of this research is to model the generation and propagation of rain-triggered landslides with a focus on small to large deformations. The modeling will be carried out in two stages: i) Modeling of a transitional stage of rainfall and infiltration using the finite element method (FEM) with CODEBRIGHT software, until conditions of non-convergence are generated due to the triggering of the fault, and ii) Modeling of the propagation of the unstable mass using the material point method (MPM), allowing large deformations to be reproduced based on the pore pressure and saturation conditions reached in the failure stage.

For phase 1 in the modeling of rain infiltration and pore pressure generation, statistically defined rain thresholds will be used. In this case, a threshold from the early warning system of Medellín and Valle de Aburrá will be used. These types of thresholds for early warning purposes basically demarcate a limit between specific weather conditions with which there is a greater possibility, in this case, of mass movements being generated. Given that the generation of mass movements does not depend on a single variable, these types of thresholds become more accurate tools when it comes to local data analysis, but their accuracy is lower when it comes to regional analysis or even for larger areas. The Medellín and Aburrá Valley Early Warning System (SIATA by its acronym in spanish) had data from 801 mass movement events for the construction of the rainfall threshold, covering the period 2013-2023, in addition to data from 40 rain gauges with 1-minute resolution.

Rain thresholds become a powerful early warning tool, as well as providing a good approximation of the conditions that trigger mass movement in specific areas. These are low-cost tools when compared to the cost of human resources, equipment, and operations required for instrumentation of slopes in large areas. Therefore, it is hoped that a

methodology can be developed that allows thresholds to be used in specific areas for risk analysis, mainly in densely populated

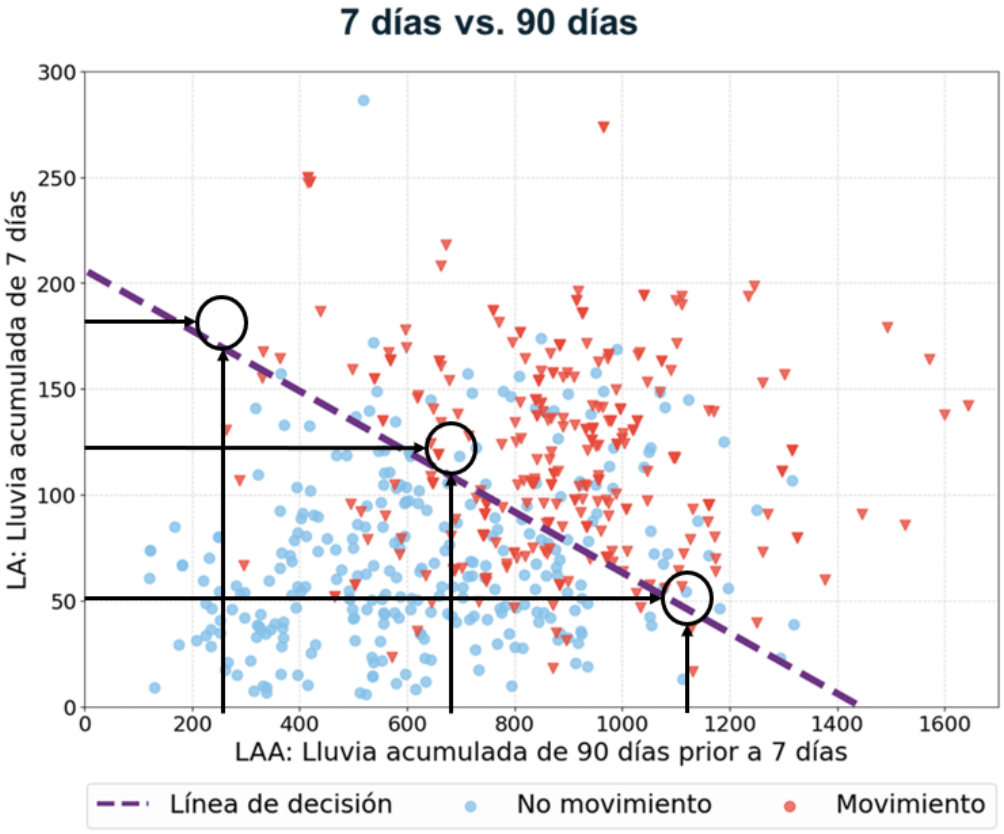

Figure 6: SIATA threshold zones selected for input parameterization in the FEM–MPM modeling framework

The SIATA rainfall threshold combines accumulated rainfall or rainfall history over 90 days (long term) and accumulated rainfall over 7 days (short term and prior to mass movement). This can be seen in Figure 6 Three (3) specific threshold zones have been selected from this threshold. The first zone has low previous rainfall and a large accumulation of triggering rainfall in the last 7 days, which has caused mass movements. A zone at the far right of the threshold with a large accumulation of previous rainfall over 90 days, whereby mass movements were triggered by low triggering rainfall in the last 7 days. Additionally, values in the intermediate zone of the threshold were selected.

With the data reported in Table 2,a mass flow condition will be imposed on the finite element model until non-convergence is reached. From this point on, the soil mass begins to break up, and the liquid pressure and stress data in the soil mass will be taken and exported as the starting point for modeling using the material point method. An important aspect to highlight is that CODEBRIGHT (FEM software) allows the export of liquid pressure data at the nodes. Therefore, prior to exporting the data to Anura3D (MPM software), it was necessary to perform linear interpolation to transfer data from the nodes to the Gauss points in the FEM environment. However, for stress data, which corresponds to element variables and not node variables, it was not necessary to perform

Table 2: Rainfall data for the selected threshold zones

Threshold Zone	Period	Rainfall (mm)	Days	Rainfall (kg/m²·s)
Zone 1	Antecedent	250	90	3.22E-05
	Triggering	175	7	2.89E-04
Zone 2	Antecedent	750	90	9.65E-05
	Triggering	125	7	2.07E-04
Zone 3	Antecedent	1150	90	1.48E-04
	Triggering	50	7	8.27E-05

any calculations on them.

6. Results

This chapter will show in detail the results obtained during the modeling performed, their analysis, and specific details considered relevant to those results.

6.1 Numerical Modeling of Rainfall Infiltration

The imposition of a mass flow is proposed to simulate rainfall infiltration, for which the CODEBRIGHT finite element software was used, a geological model with the geometry, boundary conditions, and materials as shown in Figure 3. For nomenclature purposes, the three cases from the three areas of interest in the rainfall threshold have been named Zone 1, Zone 2, and Zone 3.

The displacement contours obtained during the rain infiltration stage until model non-convergence will be presented below (see figure 7). In the case of Zone 1 of the threshold, failure occurred after 96 days; for Zone 2, after 13 days; and for Zone 3, after 6 days of rainfall infiltration. Prior to conducting other analyses, these results show that the specific soils evaluated are more susceptible to mass movements when subjected to high precipitation events in the 90 days preceding rainfall. This highlights that failures occurring within a few days of rainfall, as in Zones 2 and 3, are mainly associated with surface failures.

From finite element modeling, it is also possible to obtain the contours of pore pressures (see figure 8) that have been generated during the transient modeling of rain infiltration. On the slope subjected to the infiltration of a mass flow, in this case water, it is possible to see the deepening of the saturation front from the infiltration surface. Additionally, the liquid pressures of the water table located 3.0 m from the base of the model can be seen, as well as the effect of suction in the central area of the soil mass, which is still partially saturated.

In the case evaluated for zone 1 of the threshold, a greater deepening of the saturation

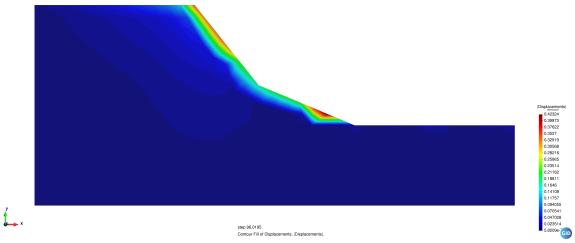

(a) Threshold Zone 1

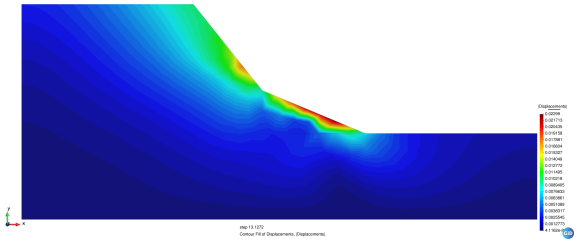

(b) Threshold Zone 2

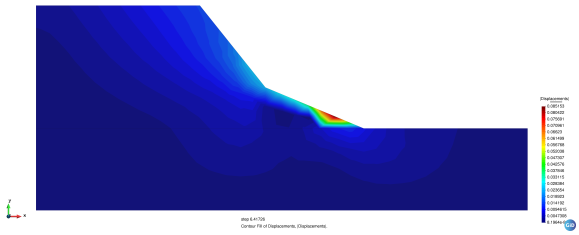

(c) Threshold Zone 3

Figure 7: Displacements obtained for the different threshold zones analyzed using CODEBRIGHT

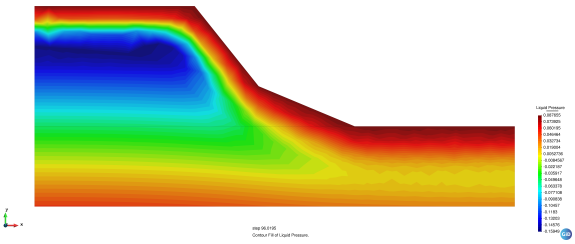

(a) Threshold Zone 1

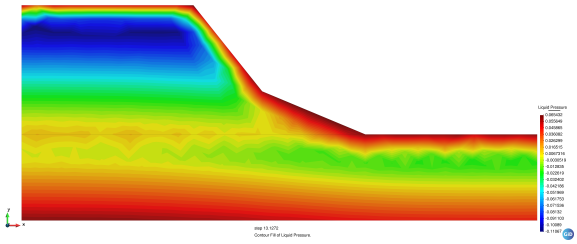

(b) Threshold Zone 2

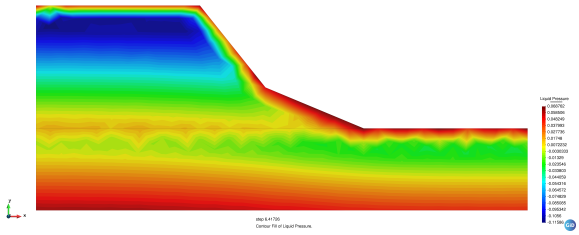

(c) Threshold Zone 3

Figure 8: Liquid pressures for the different threshold zones evaluated with the CODEBRIGHT software

front is observed, associated with the modeling of a longer infiltration time in the soil mass. Similarly, the degree of saturation is much greater around the entire contour of the saturation front. (see figure 9). It is important to note that the modeling performed up to this point corresponds to a fully coupled hydro-mechanical (HM) analysis, in which flow and deformation are analyzed simultaneously.

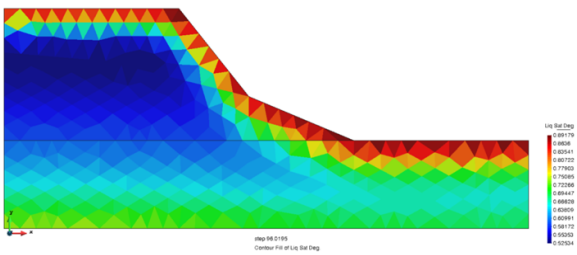

(a) Threshold Zone 1

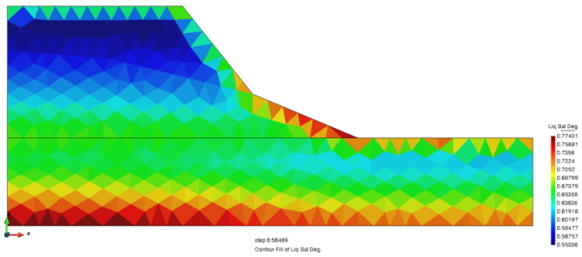

(b) Threshold Zone 2

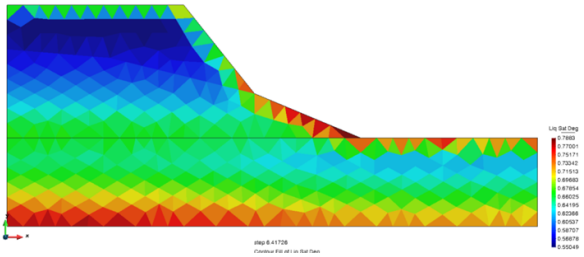

(c) Threshold Zone 3

Figure 9: Degree of saturation in the different threshold zones evaluated with the CODE$_B RIGHT software$

With the execution of the modeling carried out using the finite element method for the three (3) SIATA rainfall threshold zones, particularities are evident, such as the time elapsed before non-convergence in the numerical analysis: for zone 1, a rainfall infiltration modeling time of 96 days; for zone 2 of 6.5 days, and for zone 3 of 5.4 days, which initially shows a greater susceptibility of soils to periods of intense rainfall with high accumulation and recharge of liquid in the soil interstices.

Considering the results, in zone 1 of the threshold, there was low accumulated rainfall over 90 days, the soil mass behaved better, allowing 90 days of recharge and generation of pore pressures on the slope, with mass movement finally being triggered after 96 days by relatively high rainfall. For the other two zones of the threshold, a higher accumulated rainfall was imposed on the model in the first phase of transient modeling (initial 90 days). However, the soil mass, with the parameters selected for modeling it on the synthetic slope, reached a point of convergence, so it was not possible to continue with the modeling.

6.2 Modeling of landslide runout

After performing the finite element analyses, a model is generated under the same geometric conditions and with the same computational background mesh. For this purpose, the Anura3D code in GID is used, hereinafter referred to as GID. The stress values in X, Y, XY, and liquid pressures located at their respective Cartesian coordinates are taken to use this data as the starting point in the analysis using the material point method (MPM). The states shown in Figure 9, Figure 10, and Figure 11 correspond to the point of non-convergence in the FEM analysis, where theoretically the soil mass has entered into failure.

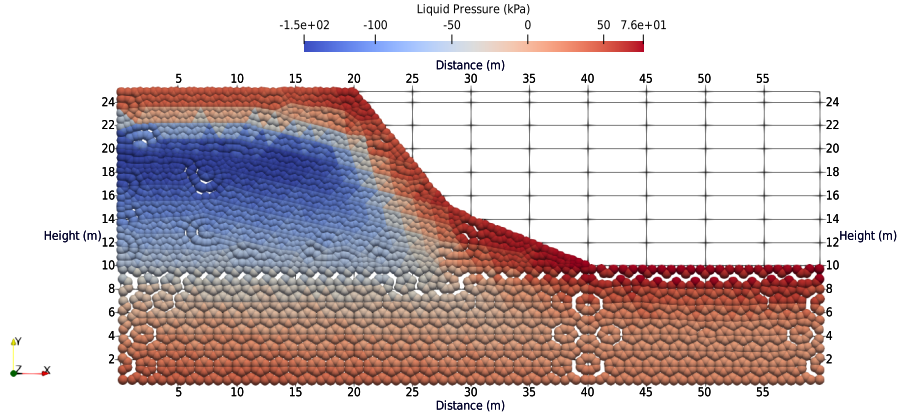

Figure 10: Initial liquid pressure conditions in the MPM model, defined by the transfer of data obtained from the FEM simulations

In the figure 10 It is possible to see how the final condition modeled in FEM, just before failure or non-convergence, is imported as the initial condition for a model in MPM. A saturation front with high pore pressures (see red zone) is evident in the soil mass of the synthetic slope, compared to a partially saturated central area (see blue zone) with the presence of suction. Similarly, positive pore pressures are evident at the base of the model, corresponding to the imposition of an initial groundwater level condition in that area of the slope.

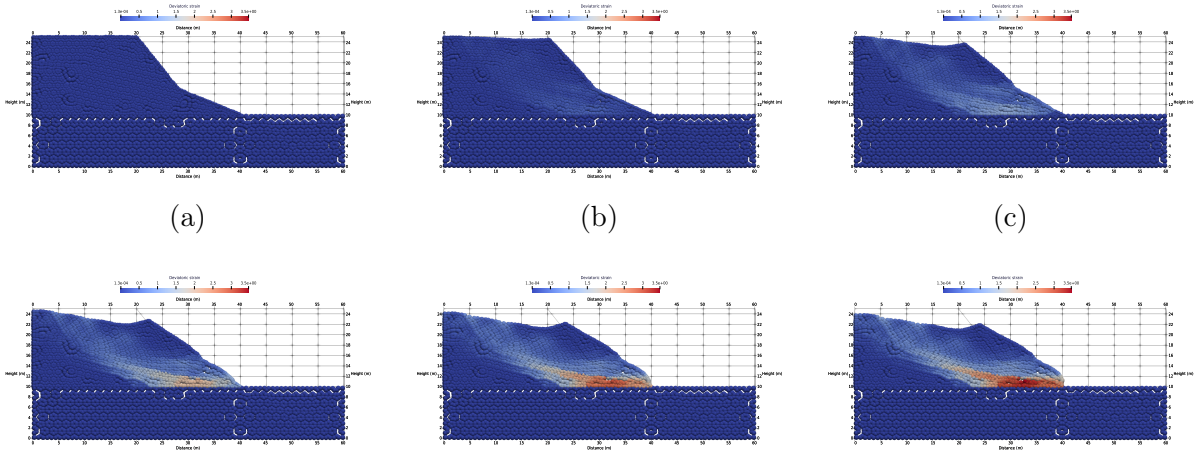

(a) (b) (c)

(d) (e) (f)

Figure 11: Deviatoric strain on the slope evaluated using information from zone 1 of the threshold in the stages following the failure: a) t=0s, b) t=10s, c) t=20s, d) t=30s, e) t=40s, f) t=50s

The failure mechanism shown in Figure 11 corresponds to a typical failure of fine materials such as clays or silts that have been subjected to a long period of water accumulation in the interstices and the generation of pore pressures. In this case, although large deformations have been triggered, the area that fails does not show a considerable runout distance.

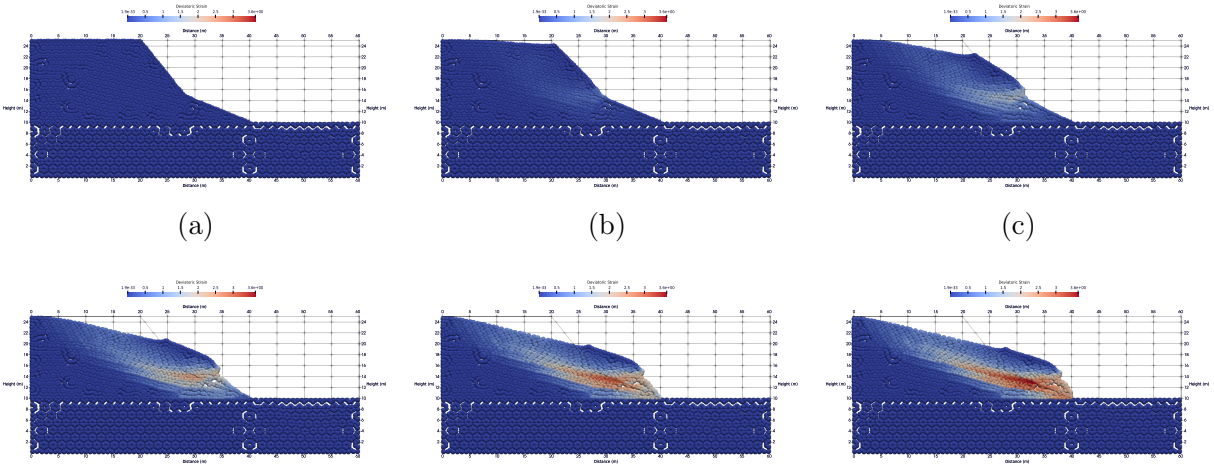

Figure 12: Deviatoric strain on the slope evaluated using information from zone 2 of the threshold in the stages following the failure: a) t=0s, b) t=10s, c) t=20s, d) t=30s, e) t=40s, f) t=50s

In contrast to the failure mechanism shown in Figure 11 cwhich corresponds to zone 1 of the SIATA rainfall threshold and involves slope failure that only moves to the accumulation zone of the first change in slope of the synthetic slope, zones 2 and 3, see figure12 and figure 13 respectively, showed greater travel distances of the mobilised mass. These were approximately 13.0 m and 12.0 m for zones 2 and 3 of the threshold.

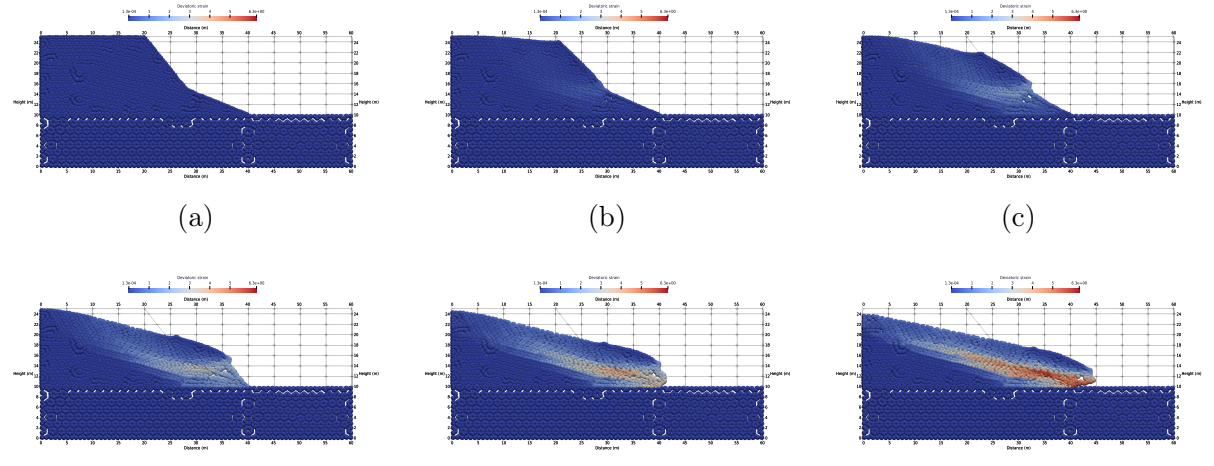

Figure 13: Deviatoric strain on the slope evaluated using information from zone 3 of the threshold in the stages following the failure: a) t=0s, b) t=10s, c) t=20s, d) t=30s, e) t=40s, f) t=50s

The selected synthetic slope geometry and the obtained failure mechanism are not far from reality; they can be likened to a road embankment that has failed due to constant rain infiltration at a certain time of year and the particular geology of the area. This type of semi-circular and deep failure is common for fine materials. In granular materials, more superficial and translational mass movements are to be expected for this type of rainfall

conditions that were imposed.

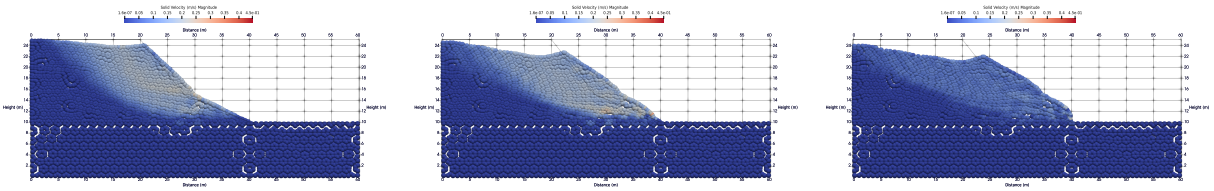

(a) (b) (c)

Zone 1 of the threshold, landslide velocity at 15 sec, 30 sec and 45 sec

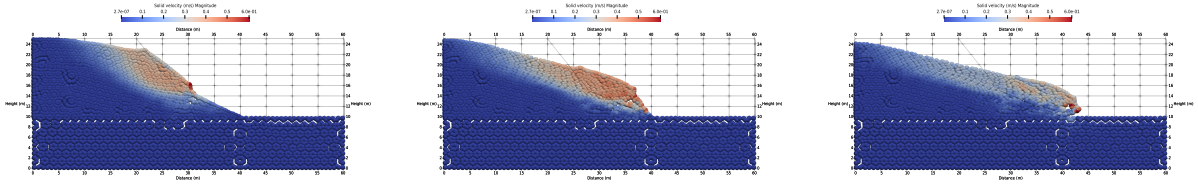

(d) (e) (f)

Zone 2 of the threshold, landslide velocity at 15 sec, 30 sec and 45 sec

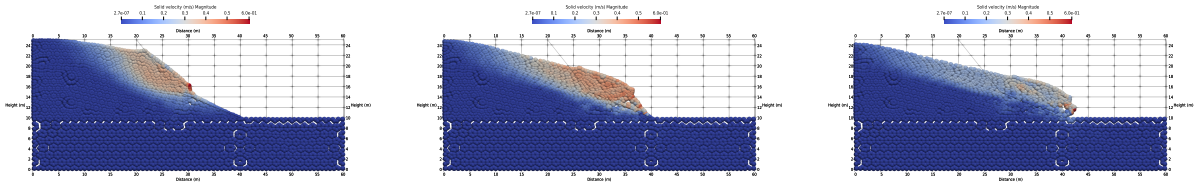

(g) (h) (i)

Zone 3 of the threshold, landslide velocity at 15 sec, 30 sec and 45 sec

Figure 14: Velocity of solids in numerical modelling for different zones of the threshold.

When plotting the values of soil mass velocity at failure with respect to time (see figure 15), we observe that, for zone 1 of the threshold, failure occurs at a relatively slower velocity than in zones 2 and 3, because in sector 1 there was a longer rain infiltration time, of approximately 96 modeling days until failure. However, in the case of zones 2 and 3, with high preceding rainfall imposed as a mass flow, failure occurred over a period of between 6 and 13 days, with maximum propagation velocities of between 0.34 and 0.39 m/s, unlike zone 1 of the threshold, where the maximum velocity was 0.22 m/s.

7. Conclusions and Limitations

The software used for modeling in this research has been developed over a long period of time and is well documented, and is available for free use (open access). For the CODEBRIGHT and Anura3D programs, there are forums where questions can be asked and contributions made to the community that uses them, so this type of FEM/MPM numerical modeling software is considered accessible. The CODEBRIGHT software code is assembled and available for download on the website of the Department of Civil and

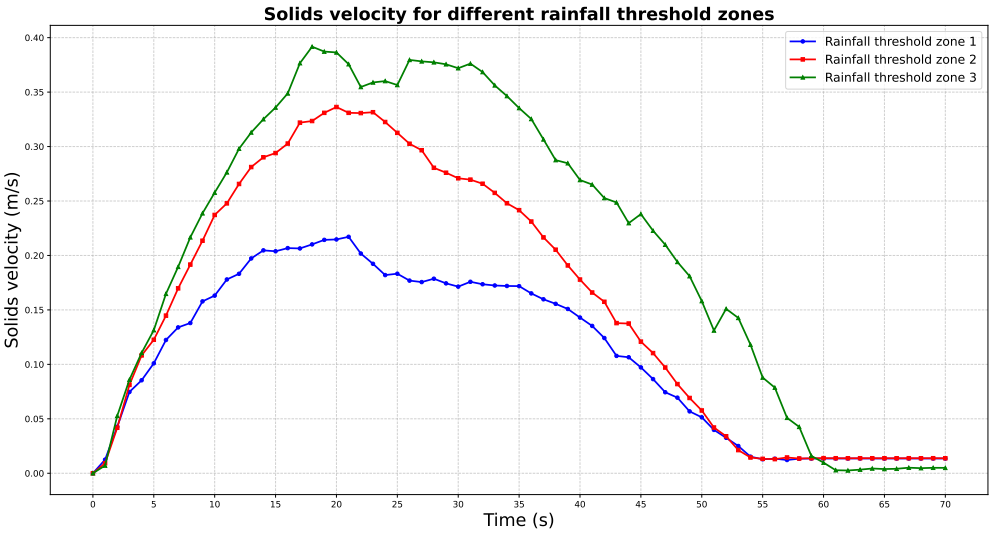

Figure 15: Variation in landslide velocity over time for the different areas of the threshold evaluated.
Source: Author's elaboration.

Environmental Engineering at the Polytechnic University of Catalonia. The Anura3D code is available on the developers' GitHub and can be compiled in Visual Studio on a conventional computer.

The synthetic slope models were created using a hydromechanical coupling analysis, in which the flow and deformation equations are solved. This analysis allows us to get closer to the actual response conditions expected for the soil mass, especially when dealing with soft soils, such as those modeled in this research. In soils with a higher modulus of rigidity and better mechanical strength, a hydro-mechanically coupled model may not differ greatly from a model that only analyzes the deformation of the soil mass.

With the two-stage modeling approach implemented, the computational efficiency of a transient analysis coupled hydromechanically with FEM is leveraged with modeling times of between 10 and 15 minutes on a conventional computer. Next, the information from the stress and liquid pressure fields just before non-convergence (failure) is taken and simulated with MPM. Performing MPM modeling of the soil saturation stage for long infiltration times, such as those considered in a rainfall threshold (97 days), requires computers with special characteristics. Even with computers with these characteristics, modeling times would be relatively long.

The materials evaluated corresponded to surface soils with a typical weathering profile from the area near the city of Medellín (Colombia), mainly fine soils (silts and clays) with medium to high compressibility. The failure mechanisms obtained were consistent with these materials: failures similar to a logarithmic spiral, for which it is possible to observe the areas of greatest shear deformation. In these areas, with maximum shear deformation, there is no longer any volumetric change, which is known as the critical state. It is understood that the failures obtained are undrained failures.

The modeling performed reproduced the behavior of the soil mass after failure, using a plane deformation model, highlighting one of the many advantages of the Anura3D code, which is the initialization of stresses by imposing the final data obtained from the FEM analysis. The data mentioned for the start of the MPM analysis correspond to stresses (X, Y, XY) and liquid pressures, for which it is not necessary for these points to coincide with the location of the material points or nodes of the computational mesh, since Anura3D interpolates the stresses to the specific location of the material points using the Kernel interpolation. However, it is extremely important to import the X-Y coordinates and the size of the mesh elements.

Horizon V basically behaved like a rock substrate, in this case due to the difference in rigidity, which is why the fault was generated in Weathering Horizon VI, corresponding to the material found on the surface and where the saturation front mainly deepened.

In real cases of risk management using this type of methodology, one of the aspects that contributes most to statistical variability and uncertainty is the parameters of the soil to be evaluated, as well as particular fluctuations in the water table and external conditions due to anthropogenic action. Nevertheless, it becomes a fairly reliable modeling alternative for estimating the possible path of a soil mass that could break or for calibrating previously generated landslides.

For the analyses performed, initial liquid pressure conditions were imposed on the synthetic slope in order to simulate a water table at 3.0 m from the base of the slope. Consequently, it was possible to observe how the saturation front gradually approached in depth while there was still an area with negative liquid pressures due to the presence of suction in a partially saturated soil.

In fine surface soils, slow failure behavior and short runout distances were observed for long periods of accumulation and infiltration prior to failure. However, failures were observed in less time, with higher propagation speeds and greater runout distances in cases with high rainfall infiltration over short periods of time.

References

[1] P. E. Aristizábal, H. Martínez, and J. I. Vélez, "Una revisión sobre el estudio de movimientos en masa detonados por lluvias," *Rev. Acad. Colomb. Cienc.*, vol. 34, 6 2010. [Online]. Available: www.emdat.be

[2] P. Das, D. Patwa, G. Vishnu, and T. V. Bharat, "Influencing factors on the simulation of rainfall-induced landslide prediction based on case study," *Bulletin of Engineering Geology and the Environment*, vol. 81, 5 2022.

[3] R. J. Marín, E. García, and E. Aristizábal, "Rainfall thresholds for shallow landslides based on physical models: Application in a sub-basin of the valle de aburrá (colombia)," *DYNA (Colombia)*, vol. 86, pp. 312–322, 7 2019.

[4] W. Zhou, H. Qiu, L. Wang, Y. Pei, B. Tang, S. Ma, D. Yang, and M. Cao, "Combining rainfall-induced shallow landslides and subsequent debris flows for hazard chain prediction," *Catena*, vol. 213, 6 2022.

[5] Y. Chong, G. Chen, X. Meng, S. Bian, F. Huan, L. Lin, D. Yue, Y. Zhang, and F. Guo, "Formation mechanism and quantitative risk analysis of the landslide-induced hazard chain by an integrated approach for emergency management: A case study in the bailong river basin, china," *Catena*, vol. 233, 12 2023. [Online]. Available: https://www.sciencedirect.com/science/article/abs/pii/S0341816223006136

[6] D. M. Cruden, "Landslide types and processes," 1 1996. [Online]. Available: https://www.researchgate.net/publication/209802944

[7] J. Hou, M. Dou, Y. Zhang, J. Wang, and G. Li, "An evaluation model for landslide and debris flow prediction using multiple hydrometeorological variables," *Environmental Earth Sciences*, vol. 80, 8 2021.

[8] F. Guzzetti, S. Peruccacci, M. Rossi, and C. P. Stark, "The rainfall intensity-duration control of shallow landslides and debris flows: An update," *Landslides*, vol. 5, pp. 3–17, 2 2008.

[9] M. Lu, F. Ceccato, M. Zhou, A. Yerro, and J. Zhang, "Evaluating the exceedance probability of the runout distance of rainfall-induced landslides using a two-stage fem-mpm approach," *Acta Geotechnica*, vol. 19, pp. 3691–3706, 6 2024.

[10] Y. Thiery, H. Kaonga, H. Mtumbuka, M. Terrier, and J. Rohmer, "Landslide hazard assessment and mapping at national scale for malawi," *Journal of African Earth Sciences*, vol. 212, 4 2024.

[11] D. V. Griffiths, G. A. Fenton, and N. Manoharan, "Bearing capacity of rough rigid strip footing on cohesive soil: Probabilistic study," *Journal of Geotechnical and Geoenvironmental Engineering*, vol. 128, pp. 743–755, 9 2002.

[12] J. M. Duncan, "State of the art: Limit equilibrium and finite-element analysis of slopes," *J. Geotech Engrg*, vol. 122, 7 1996.

[13] D. V. Griffiths and P. A. Lane, "Slope stability analysis by finite elements," *Géotechnique*, vol. 51, pp. 653–654, 9 2001.

[14] D. A. Bouzid, "Finite element analysis of slope stability by expanding the mobilized principal stress mohr's circles – development, encoding and validation," *Journal of Rock Mechanics and Geotechnical Engineering*, vol. 14, pp. 1165–1179, 8 2022.

[15] J. L. G. Acosta, P. J. Vardon, and M. A. Hicks, "Study of landslides and soil-structure interaction problems using the implicit material point method," *Engineering Geology*, vol. 285, 5 2021.

[16] J. L. G. Acosta, P. J. Vardon, G. Remmerswaal, and M. A. Hicks, "An investigation of stress inaccuracies and proposed solution in the material point method," *Computational Mechanics*, vol. 65, pp. 555–581, 2 2020.

[17] L. Beuth and T. B. P. A. Vermeer, "Large deformation analysis using a quasi-static material point method." *Journal of Theoretical and Applied Mechanics*, vol. 38, 10 2008. [Online]. Available: https://www.sciencedirect.com/science/article/abs/pii/S0341816223006136

[18] F. H. Harlow and B. D. Meixner, "The particle-and-force computing method for fluid dinamics," 10 1961.

[19] M. A. Llano-Serna and M. M. Farias, "Validación numérica, teórica y experimental del método del punto material para resolver problemas geotécnicos," *Revista Internacional de Metodos Numericos para Calculo y Diseno en Ingenieria*, vol. 32, pp. 110–115, 4 2016.

[20] S. G. Bardenhagen and E. M. Kober, "The generalized interpolation material point method," pp. 477–495, 2004.

[21] D. Sulsky, Z. Chenb, and H. L. S. ¢', "A particle method for history-dependent materials," pp. 179–196, 1994.

[22] S. Bardenhagen, "The material-point method for granular materials," 7 1998.

[23] D. Sulsky, "Application of a particle-in-cell method to solid mechanics," *Comput. Phys. Commun*, vol. 96, pp. 105–106, 3 1996.

[24] O. Buzzi, D. M. Pedroso, and A. Giacomini, "Caveats on the implementation of the generalized material point method," pp. 85–106, 2008.

[25] Z. Wickowski, "The material point method in large strain engineering problems," *Computer Methods in Applied Mechanics and Engineering*, vol. 193, pp. 4417–4438, 10 2004.

[26] E. E. Alonso, A. Yerro, and N. M. Pinyol, "Recent developments of the material point method for the simulation of landslides," in *IOP Conference Series: Earth and Environmental Science*, vol. 26. Institute of Physics Publishing, 9 2015.

[27] N. Pinyol, J. Vaunat, and E. Alonso, "Landslides in reservoirs. a coupled thermo-hydro-mechanical approach," 9 2010. [Online]. Available: http://www.tdx.cat/TDX-0127111-095429

[28] A. Yerro, E. Alonso, and N. Pinyol, "Modelling progressive failure with mpm," in *Numerical Methods in Geotechnical Engineering - Proceedings of the 8th European Conference on Numerical Methods in Geotechnical Engineering, NUMGE 2014*, vol. 1. Taylor and Francis - Balkema, 2014, pp. 319–323.

[29] Y. Zhu, T. Ishikawa, Y. Zhang, B. T. Nguyen, and S. S. Subramanian, "A fem-mpm hybrid coupled framework based on local shear strength method for simulating rainfall/runoff-induced landslide runout," *Landslides*, vol. 19, pp. 2021–2032, 8 2022.

[30] C. Ying, K. Zhang, Z. N. Wang, S. Siddiqua, G. M. H. Makeen, and L. Wang, "Analysis of the run-out processes of the xinlu village landslide using the generalized interpolation material point method," *Landslides*, vol. 18, pp. 1519–1529, 4 2021.

[31] X. Liu and Y. Wang, "Probabilistic simulation of entire process of rainfall-induced landslides using random finite element and material point methods with hydro-mechanical coupling," *Computers and Geotechnics*, vol. 132, 4 2021.

[32] S. Olivella, J. Carrera, A. Gens, and E. E. Alonso, "Nonisothermal multiphase flow of brine and gas through saline media," *Transport in Porous Media*, vol. 15, pp. 271–293, 6 1994.

[33] I. Jassim, D. Stolle, and P. Vermeer, "Two-phase dynamic analysis by material point method," *International Journal for Numerical and Analytical Methods in Geomechanics*, vol. 37, pp. 2502–2522, 10 2013.

[34] G. Duan, F. Song, A. Rodríguez-Dono, L. Wang, and J. Chen, "Stability analysis of unsaturated loess slopes subjected to extreme rainfall incorporating creep effects," *Computers and geotechnics*, vol. 169, 3 2024.